Acoustically Triggered Harvesting of Nanometer Airborne Particles – A Numerical Model for the Ultrasonic Manipulation

D Rubinetti*, D A Weiss
Institute of Thermal and Fluid Engineering, University of Applied Sciences and Arts Northwestern Switzerland

ABSTRACT
In this study, the focus is to model the physics of acoustic harvesting for 100 nanometer particles in order to lay the groundwork for technical feasibility studies. Based on a simplified 2D test-case channel geometry with an intense acoustic standing wave field the relevant drag and acoustic forces are reviewed and implemented in a numerical model. The standing wave is appropriately formulated to harvest particles in one single pressure antinode which conforms to the centerline of the channel. The particle trajectories along the chosen test-case channel have been analytically verified. Advancements in the acoustic manipulation of particles have mainly received attention for liquid carrier media. The conceived model is numerically stable and suitable to assess the potential of harvesting nanometer aerosols in gaseous environments.

1. INTRODUCTION

Acoustic harvesting denotes the effect of accumulating e.g. airborne nanometer particles in a standing wave field. In life sciences and medical applications the use of intense acoustic fields at frequencies typically of the order of several kHz is a mature and well-established technique to manipulate the trajectory of a particle in a liquid carrier medium. The method is capable of separating particles such as blood cells from a continuous stream [2].

The adaptation to gaseous carriers is a promising approach to enhance the control of particle emissions. Renewable energy sources such as wood and biomass produce significant amounts of fly ash during combustion with particle diameters typically in the realm of nanometers. Conventional separation techniques such as the electrostatic precipitation have excellent filtration efficiency for micron-sized particles [1], whereas smaller particles are more difficult to capture. Moreover, such particles pose a considerable health hazard due to their capability to penetrate the respiratory system.

Acoustic harvesting has received attention as pretreatment stage of a conventional particle removing device to improve coagulation [2]. In this study the physical framework for a continuous sorting of particles in a flow-through channel is constructed and investigated numerically. The investigation is described and carried out by means of a 2D test-case channel geometry of 35mm x 4mm.

*Corresponding Author: donato.rubinetti@fhnw.ch

2. PHYSICAL MODEL

The nature of acoustic harvesting is a true multiphysics problem due to the coupling of acoustics, fluid flow and particle dynamics. Figure 1 illustrates the interactions involved in an acoustic harvesting process.

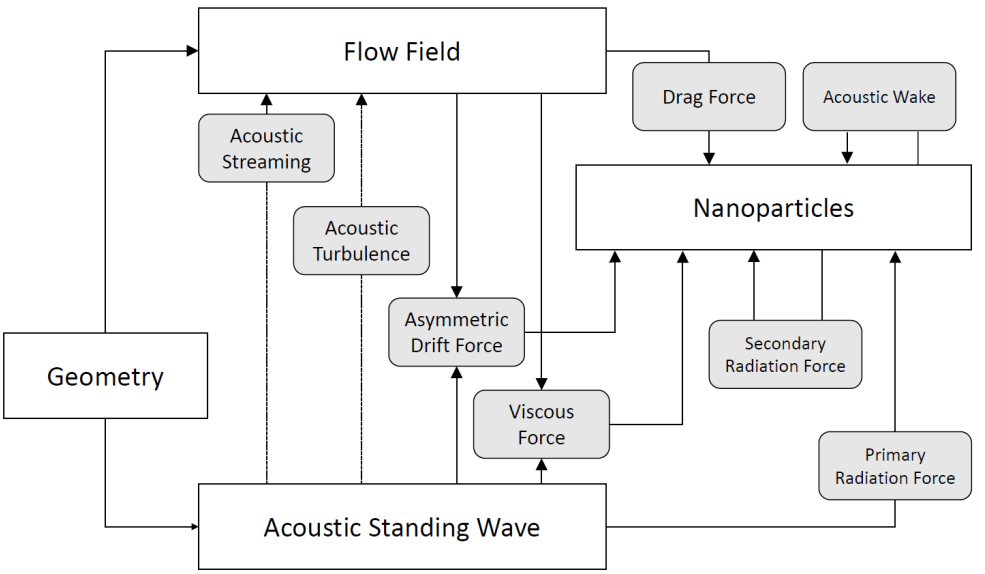

Figure 1: Coupled physics in an acoustic harvesting system for nanometer particles. The interactions between the different fields (flow field, acoustic standing wave and dynamic particle field) are highlighted by the corresponding physical phenomenon. Acoustic streaming and acoustic turbulence are believed to have only weak influence [4]. In this study, the acoustic wake effect and secondary radiation force as particle-particle interaction forces are not implemented.

Acoustic streaming is an effect inducing a steady flow in the fluid due to the absorption of ultrasound waves. It has been intensively studied in previous analyses for liquid carrier media and is neglected in the present work [3]. The second nonlinear effect, acoustic turbulence, has been considered to be insignificant for the agglomeration process [4].

The remaining interactions illustrated in Figure 1 are described by means of an analytically verifiable 2D test-case for 100 nm soot particles.

2.1. Test-Case Geometry

The numerical model is developed for a 2D channel according to Figure 2. The fluid is air at standard conditions with the speed of sound of $c_0 = 343\ \mathrm{m/s}$. The propagation direction of acoustic waves is perpendicular to the direction of the initial velocity field. Hence, particles are driven towards the center of the channel in the pressure antinode of the standing wave. In this setup, the frequency of the ultrasound field is $f = {}^{c_0}/_{\lambda} = 42.9\ \mathrm{kHz}$. This corresponds to a wavelength of the ultrasound of $\lambda = 8\ mm$, i.e. twice the channel height L. The particles enter the domain embedded in a fully developed laminar flow with a peak velocity of $w_{max} = 0.1\ \mathrm{m/s}$. The corresponding Reynolds number writes

$$Re = \frac{\rho_f \bar{w} L}{\mu} \tag{1}$$

with the average flow velocity $\bar{w} = \frac{2}{3} w_{max}$, the channel height $L = 4\,mm$, air density $\rho_f = 1.225\ {}^{\mathrm{kg}}/_{\mathrm{m}^3}$ and air dynamic viscosity $\mu = 1.81 \cdot 10^{-5}$ Pa · s, resulting in $Re \approx 18$ which complies with the assumption of a laminar flow pattern.

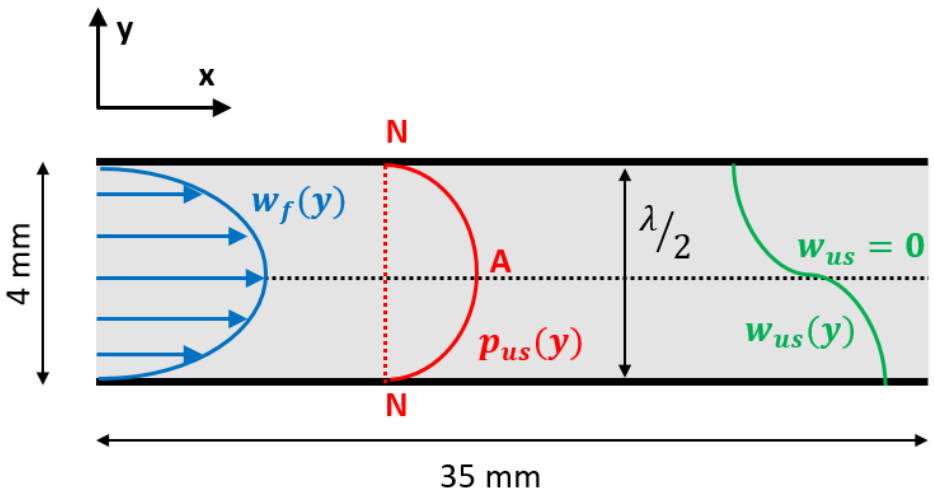

Figure 2: Sketch of the 2D test-case geometry. The height of the channel is exactly half of a wavelength, resulting in a pressure antinode (A) in the centerline of the channel and two pressure nodes. In this configuration, the harvesting of aerosols is expected to take place on the centerline

2.2. Standing Wave

Acoustic waves propagate along the y-direction forming a standing wave. Mathematically, the standing wave is described by

$$p_{us}(y) = p_a \cos(ky) \tag{2}$$

with the pressure amplitude $p_a = 5000$ Pa and the wavenumber $k = {}^{2\pi}/_{\lambda}$. The coordinate y is thereby reckoned from the centerline. Note that the indicated pressure amplitude corresponds to a huge sound pressure level (SPL) of 160-180 dB. The convenience of such elevated pressure amplitude is that particles can easily be displaced for testing purposes. The acoustic velocity can be derived with respect to the phase shift and is

$$w_{us}(y) = \frac{p_a}{c_0 \rho_f} \sin(ky) \tag{3}$$

2.3. Primary Radiation Force

The primary radiation force directly couples the acoustic field to the dynamics of the particles. The displacement occurs in wave propagation direction as ultrasound submitted particles experience the time-averaged force. In its original form, the force was derived by King [5] for a rigid sphere $\left(d_p \ll \lambda\right)$ as follows

$$F_{\mathrm{rad1}} = -\nabla V_p \left(f_1 \frac{1}{2\rho_f c_0^2} \langle {p_{us}}^2 \rangle - f_2 \frac{3}{4} \rho_f \langle {w_{us}}^2 \rangle \right) \tag{4}$$

$$f_1 = 1 - \frac{\rho_f c_0^2}{\rho_p c_p^2} = 1 - \frac{\kappa_p}{\kappa_f} = 1 - \frac{\beta_f}{\beta_p} \tag{5}$$

$$f_2 = \frac{2(\rho_p - \rho_f)}{2\rho_p + \rho_f} \tag{6}$$

where V_p stands for the particle volume, $\langle {p_{us}}^2 \rangle$ and $\langle {w_{us}}^2 \rangle$ for the time-averaged acoustic pressure and acoustic velocity, c_p for the compressional speed of sound of the particle ($\sim$1000 $^{\mathrm{m}}/_{\mathrm{s}}$), ρ_p for the particle density (here: $\rho_p = 2000$ $^{\mathrm{kg}}/_{\mathrm{m}^3}$), κ_p for the particle compressibility (here: $\frac{1}{2 \cdot 10^9}$ Pa^{-1}) and $\kappa_f = \frac{1}{\rho_f c_0^2}$ for the compressibility of air. The compressibility may be written as the inverse of the bulk moduli β_f and β_p. In this notation, the acoustic radiation force as time average does not depend on time but on space only as are the algebraic expressions for the standing wave according to Eqs. (2) and (3). Hence, for our test-case it is valid that $\langle {p_{us}}^2 \rangle = {p_{us}(y)}^2$ and $\langle {w_{us}}^2 \rangle = {w_{us}(y)}^2$.

In flow cytometry systems, i.e. for blood analysis, the liquid is submitted to an intense acoustic field (150-180 dB) where the primary radiation force dominates the alignment of suspended micron-size particles. However, in airborne systems with considerably smaller particles (nanometers) further forces need to be modeled to accurately represent agglomeration. The reason is that the primary radiation force derived by King [5] assumes that the fluid surrounding the particle is inviscid. This assumption is valid for particles where the viscous boundary layer formed around the particle is much smaller than the particle diameter itself. Here, the viscous boundary layer thickness δ_s is estimated by

$$\delta_s = \sqrt{\frac{2\nu}{\omega}} \tag{7}$$

with the kinematic viscosity $\nu = {}^{\mu}/_{\rho_f}$ and the angular frequency $\omega = 2\pi f$ which results in $\delta_s = 10$ µm. Consequently, the inviscid assumption for 100 nm particles does not hold and viscous effects such as the viscous force and the asymmetric drift force need to be taken into account to predict the displacement of nanoparticles submitted to ultrasound.

2.4. Secondary Radiation Force

The secondary radiation force is a particle-particle interaction arising from the scattered waves of the incident wave field. Weiser et al. [6] derived an expression for the secondary radiation force between two oscillating solid spheres in a fluid in radial coordinates as

$$F_{\mathrm{rad2}}^{r} = F_0(3\cos^2(\theta) - 1) \tag{8}$$

$$F_{\mathrm{rad2}}^{\theta} = F_0 \sin(2\theta) \tag{9}$$

$$F_0 = \frac{2\pi(\rho_p - \rho_f)^2 {w_{us}}^2 {d_{p1}}^3 {d_{p2}}^3}{3\rho_f r^4} \tag{10}$$

where d_{p1} denotes the diameter of particle 1 and d_{p2} the diameter of the second particle 2, while the distance between the particle centers is r. Figure 3 illustrates the actuation principle of the secondary radiation force. Depending on the orientation of two particles, the azimuthal force $F_{\mathrm{rad2}}^{\theta} = F_\theta$ and radial force $F_{\mathrm{rad2}}^{r} = F_r$ continuously change direction, thus, resulting in mutual attraction or repulsion.

The secondary radiation force as well as the acoustic wake effect as particle-particle interactions are not part of the numerical model in this work.

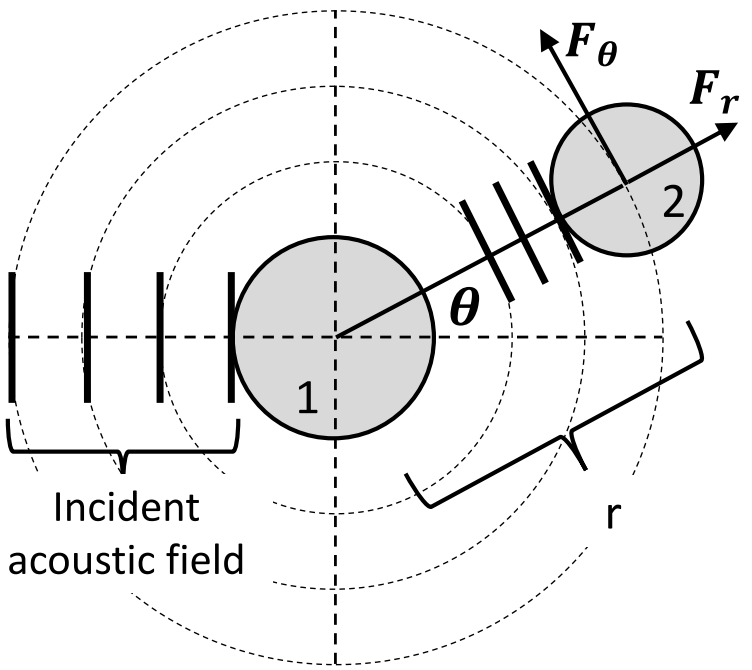

Figure 3: Secondary radiation force between two rigid spheres 1 and 2 separated by distance r. The incident acoustic field hits sphere 1 and scatters the field onto sphere 2.

2.5. Viscous Force

The primary radiation force assuming an inviscid fluid is complemented by the viscous force resulting in a significant increase of the radiation force for particle sizes smaller than the viscous boundary layer thickness δ_s [7–11]. Hence, a viscosity-dependence between acoustic

field and flow field is established. The following set of equations is required to implement the viscous force acting towards the standing wave antinode in a 1D planar standing wave:

$$F_v = \frac{3}{4}\frac{\mu\pi}{\rho_f c_0}(\chi - 3) d_p \xi_g^2 \kappa_s p_a^2 \sin(2ky) \tag{11}$$

$$\xi_g = \sqrt{1 - \xi_p^2} \tag{12}$$

$$\xi_p = \sqrt{\frac{1}{1+\omega^2\tau^2}} \tag{13}$$

$$\tau = \frac{\rho_p d_p^2}{18\mu}. \tag{14}$$

χ is the specific heat ratio, in air typically $\chi = 1.4$. ξ_g stands for the particle flow-around coefficient, ξ_p for the particle entrainment coefficient and τ for the particle relaxation time. For the present case the relaxation time is in the order of 60 ns which means that ξ_p becomes close to unity and the particle responds nearly instantaneous to external forces.

2.6. Asymmetric Drift Force

The asymmetric drift force causes a dipole oscillation within the particle, thus, leading to translational motion of the particle. This force becomes relevant for heavy $(\rho_f \ll \rho_p)$ and small particles $(d_p \ll \delta_s)$ [8,9,11]. In a 1D planar standing wave field the force acting towards the pressure antinode of the acoustic field takes the following form:

$$F_a = -\frac{\pi}{96}\kappa_s p_a^2 k d_p^3 \xi_p \left(\frac{9}{2}\xi_g(b^2 + b) + \xi_p\left(3 + \frac{9}{2}\right)\right) \sin(2ky) \tag{15}$$

Where b is defined as the ratio between boundary layer thickness and particle size $b = 2\delta_s / d_p$.

2.7. Drag Force

The drag force acting on a spherical particle in a laminar flow is suitably described by the Stokes model adjusted for nanometer particles by using the Cunningham correction factor C_c [12]. Since the particles are initiated in a fully developed laminar velocity profile the drag force acts opposite to the velocity vector.

$$F_d = \frac{3\pi\mu d_p}{C_c}(w_f - w_p) \tag{16}$$

$$C_c = 1 + \frac{\lambda_m}{d_p}\left(2.34 + 1.05\exp\left(-0.39\frac{d_p}{\lambda_m}\right)\right) \tag{17}$$

With w_f being the surrounding fluid velocity and w_p the particle velocity. λ_m is the

molecular mean free path (in air $\lambda_m \cong 66$ nm). Considering 100 nm particles in this study the Knudsen number $Kn = \frac{\lambda_m}{d_p}$ amounts to 0.66 which falls into the regime of transitional flow between free molecular flow and continuum flow. The Cunningham slip correction factor bridges this gap and ensures the validity of the continuum approach.

3. NUMERICAL MODEL

3.1. Setup

The numerical model is implemented in the commercial tool COMSOL Multiphysics. Due to the simplicity of the test-case geometry shown in Figure 2 the computational domain can be restricted to the upper half of the channel. In this study, it is imposed that there is only one-way coupling, meaning that the flow and acoustic field act on the particles but not vice-versa. Therefore, the corresponding forces can be retrieved from the underlying acoustic pressure Eq. (2) and acoustic velocity Eq. (3) without the need to solve the governing equations of linear acoustics. Analogously, instead of solving the full incompressible Navier-Stokes equations for the fluid flow the parabolic velocity field is directly specified as

$$w_f(y) = w_{max}\left(1 - \frac{y^2}{h^2}\right) \tag{18}$$

where $h = 2\ mm$ is half the height of the original channel. Figure 4 shows the computational domain used in this time-dependent study. As sampling probes 5 equally spaced 100 nm particles at $y(t = 0) = 0.2, 0.6, 1.0, 1.4, 1.8$ mm are placed at the inlet.

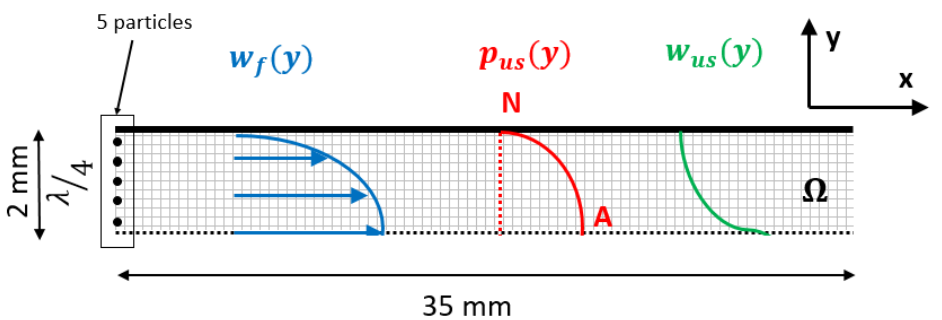

Figure 4: Sketch of the computational domain with the imposed laminar velocity profile $w_f(y)$, the ultrasound pressure $p_{us}(y)$ and the ultrasound velocity $w_{us}(y)$. At the beginning (t,x=0) of the channel a sample of 5 particles is initiated.

3.2. Particle momentum equation

The 2D particle momentum equation is derived from Newton's second law and writes

$$\frac{d}{dt}(m_p \boldsymbol{w_p}) = \boldsymbol{F_{rad1}} + \boldsymbol{F_v} + \boldsymbol{F_a} + \boldsymbol{F_d} \tag{19}$$

where the particle-particle interaction force $\boldsymbol{F_{rad2}}$ is omitted in the test-case, in order to analytically verify the particle trajectories of the computational model. $\boldsymbol{F_{rad1}}$, $\boldsymbol{F_v}$ and $\boldsymbol{F_a}$ act only in direction of the acoustic wave propagation. Thereby, $\boldsymbol{F_{rad1}}$ given by Eq. (4) simplifies to [6].

$$F_{rad1} = \left(\frac{p_a^2 V_p \kappa_s \pi}{2\lambda}\right)\left(\frac{5(\rho_p - 2\rho_s)}{(2\rho_p + \rho_s)} - \frac{\beta_p}{\beta_s}\right)\sin\left(\frac{4\pi y}{\lambda}\right) \tag{20}$$

3.3. Mesh and time-stepping

The mesh is a mapped uniform mesh with quadrilateral elements. Each element has a side-length of 0.05 mm resulting in a total amount of 28000 cells. The time-dependent solver runs from $t = 0\,\mathrm{s}$ to $t = 1\,\mathrm{s}$ with an output-writing interval of $0.01\,\mathrm{s}$. Using a fully coupled GMRES iterative solver the simulation takes 5 seconds on a mobile workstation with 32 GB RAM and 3.2 GHz processor.

4. RESULTS

4.1. Flow and acoustic fields

Figures 5 and 6 illustrate the aforementioned user-defined implementation of the flow and acoustic field. Using the centreline as a symmetry is a reasonable simplification. The parabolic velocity profile is correctly accounted for in the reduced geometry, too.

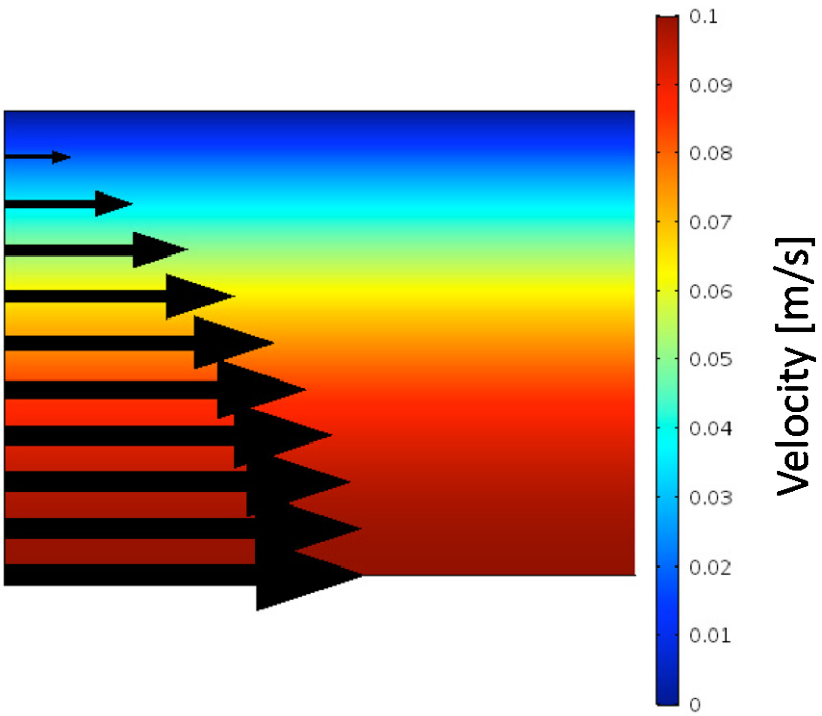

Figure 5: Velocity profile of the imposed laminar flow with profile arrows. The simplification of the geometry has its validity also for the flow field.

The curves in Figure 6 show the absolute values of the imposed ultrasound pressure and velocity across the height of the channel. Particles submitted to an acoustic ultrasound field are driven towards the pressure antinode which corresponds to an acoustic velocity of 0.

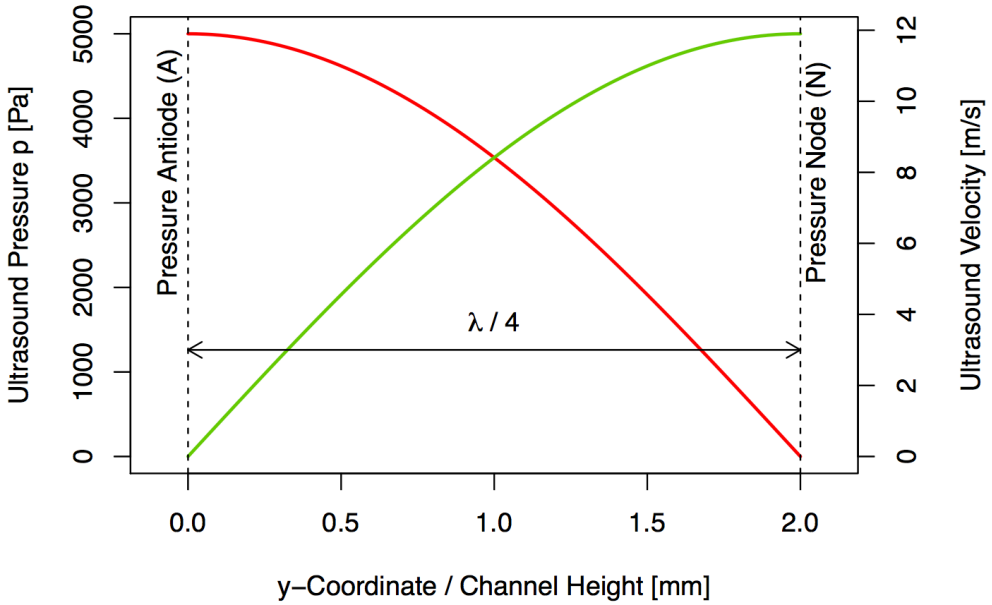

Figure 6: Imposed ultrasound pressure and velocity with absolute values over the height of the channel.

4.2. Analytical verification

By balancing the acoustic forces with the drag force an analytical expression for the particle trajectory is obtained [11,13]

$$y(t) = \frac{1}{k}\tan^{-1}(\tan(ky(t=0))\exp(2k\zeta t)) \tag{21}$$

which predicts the position of the particle at any given time t starting from the initial position of the particle $y(t=0)$. The factor ζ is setup-dependent and writes

$$\zeta = \frac{\zeta_r+\zeta_a+\zeta_v}{\zeta_d} \tag{22}$$

where its components originate from the corresponding forces for radiation force, acoustic force, viscous force and drag force, such that:

$$\zeta_r = \left(\frac{p_a^2 V_p \kappa_s \pi}{2\lambda}\right)\left(\frac{5(\rho_p-2\rho_s)}{(2\rho_p+\rho_s)} - \frac{\beta_p}{\beta_s}\right) \tag{23}$$

$$\zeta_a = -\frac{\pi}{96}\kappa_s p_a^2 k d_p^3 \xi_p \left(\frac{9}{2}\xi_g(b^2+b) + \xi_p\left(3+\frac{9}{2}\right)\right) \tag{24}$$

$$\zeta_v = \frac{3}{4}\frac{\mu\pi}{\rho_f c_0}(\chi-3) d_p \xi_g^2 \kappa_s p_a^2 \tag{25}$$

$$\zeta_d = \frac{3\pi\mu d_p}{C_c} \tag{26}$$

As a complex particle-particle interaction the secondary radiation force cannot be balanced to obtain an analytical expression. Thus, the test-case for 100 nm particles is only setup with primary radiation force, viscous force, asymmetric drift and drag force. The resulting particle trajectories show congruent agreement as shown in Figure 7. Due to the length of the channel of 35 mm the simulated particle trajectories remain at some finite constant distance from the centerline after a certain time. In the simulation, the particles have then reached the end of the channel. However, the analytical result clearly indicates that with the pressure amplitude of 5000 Pa already after a second of ultrasound exposure (which corresponds to a distance of some 0.1m along the channel) an unilinear agglomeration of particles is achieved.

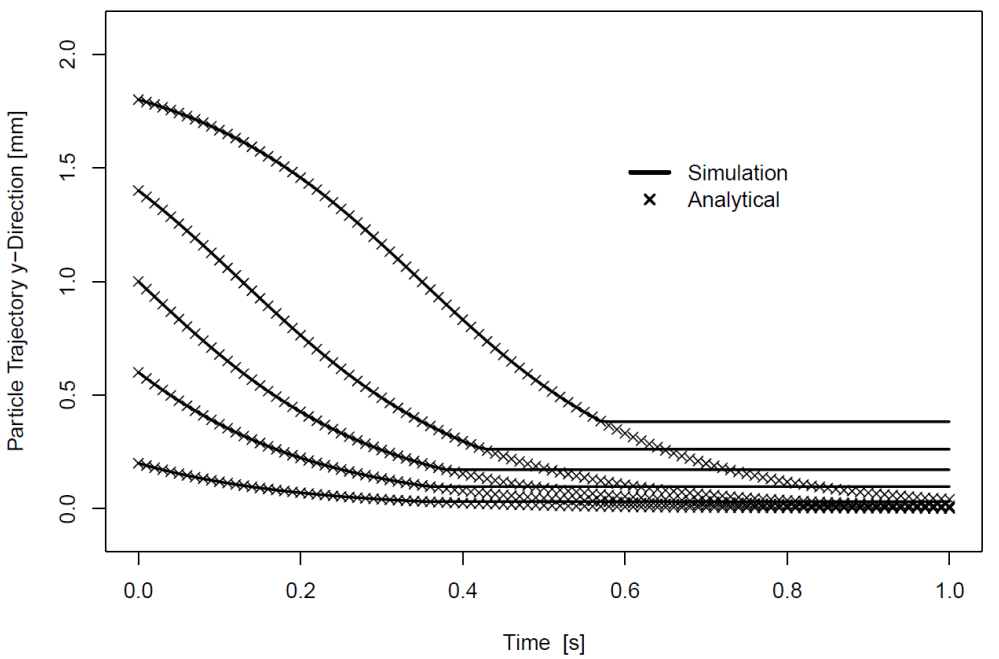

Figure 7: Variation of y-position of the particle trajectories with respect to time. The analytically calculated values and simulated results are identical. After a certain time, the simulation reaches a constant y-distance because the particles have reached the end of the computational domain. The analytical trajectories predict the development for a longer channel.

4.3 Discussion

The suggested modeling approach for acoustic harvesting of airborne particles is numerically stable and the results are analytically verified by means of a simplified test-case geometry. Experimental data for nanometer aerosols is scarcely published, and even in successful cases the retrieval poses a significant technical hurdle [11]. Therefore, an analytical verification of the modelling concept proves to be a solid basis for model extension allowing parametric studies and the assessment of technical feasibility.

Figure 8 directly compares the absolute coefficients for the acoustic forces involved in the acoustic harvesting process as a function of the particle size. The acoustic forces undergo remarkable changes. In the case of 100 nm particles the acoustic forces rank

1. Asymmetric drift force
2. Viscous force
3. Primary radiation Force

It can be shown that the primary radiation force only marginally affects the trajectories of nanometer particles submitted to ultrasound fields. The drag force coefficient has a different magnitude and cannot be directly compared.

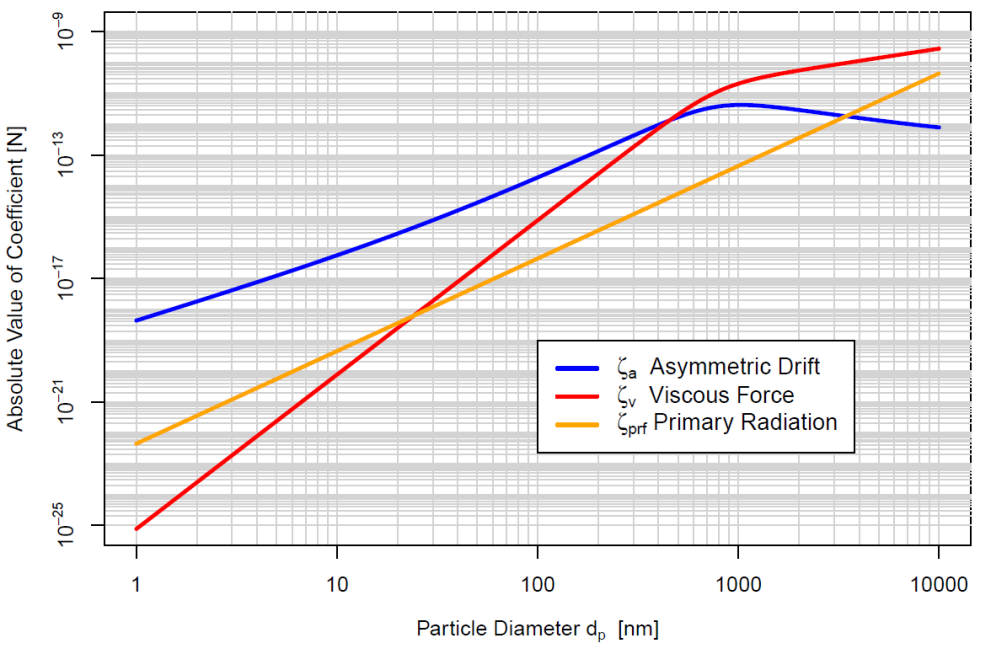

Figure 8: Comparison of the influence of acoustic and drag force contributions on different particle sizes

However, for a complete numerical setup the secondary radiation force and acoustic wake effect must be included too. Further studies will focus on the importance of the particle-particle interactions dependent on the particle size distribution and concentration, to assess the technical feasibility of acoustic harvesting devices.

5. CONCLUSION

Particle manipulation by means of intense acoustic ultrasound fields is a mature technique which is well-established in applications with a liquid carrier medium. In this study a numerical model to prove the physical feasibility of acoustic harvesting – the agglomeration of nanometer aerosols – was successfully conceived and verified. The model consists of a simple 2D channel test-case. The dynamical particle movement across the channel is influenced by the underlaying fluid velocity field and the acoustic field, respectively.

At such small dimensions experimental data is delicate to obtain. Further studies aim at studying the technical feasibility for acoustic harvesting devices.

ACKNOWLEDGEMENTS

Fruitful discussions with Ernest Weingartner are gratefully acknowledged.

REFERENCES

[1] Rubinetti D, Weiss D, Egli W, Modeling and numerical calculation concept for electrostatic precipitators, Gefahrstoffe - Reinhaltung der Luft, 2016, 76 (203). https://www.gefahrstoffe.de/gest/article.php?data[article_id]=85819

[2] Riera E, González-Gomez I, Rodríguez G, Gallego-Juárez JA, Ultrasonic agglomeration and preconditioning of aerosol particles for environmental and other applications, Power Ultrasonics, 2015, 34, 1023-1058.

[3] Rubinetti D, Weiss DA, Müller J, Wahlen A, Numerical Modeling and Validation Concept for Acoustic Streaming Induced by Ultrasonic Treatment, COMSOL Conference Munich (D) Proceedings, 2016, 2-14 Oct 2016.

[4] Tiwary R, Acoustically generated turbulence and its effect on acoustic agglomeration, J. Acoust. Soc. Am., 1984, 76 (841), 841-849.

[5] King L V, On the Acoustic Radiation Pressure on Spheres. Proc. Roy. Soc. A, 1934, 147, 212-240.

[6] Weiser MAH, Apfel RE, Neppiras EA, Interparticle Forces on Red Cells in a Standing Wave Field. Acta Acustica united with Acustica, 1984, 56, 114-119.

[7] Westerwelt PJ, The mean pressure and velocity in a plane acoustic wave in a gas, J. Acoust. Soc. Am., 1950, 22, 319-327.

[8] Czyz H, On the concentration of aerosol particles by means of drift forces in a standing wave field, Acoustica, 1990, 70, 23-28.

[9] Mednikov EP, Acoustic coagulation and precipitation of aerosols, 1963, New York: Consultants Bureau.

[10] Karlsen JT, Bruus H, Forces acting on a small particle in an acoustical field in a thermoviscous fluid, Physical Review E, 2015, 92 (4). DOI: https://dx.doi.org/10.1103/physreve.92.043010

[11] Imani RJ, Robert E, Estimation of acoustic forces on submicron aerosol particles in a standing wave field, Aerosol Science and Technology, 2018, 52 (1), 57-68. DOI: https://dx.doi.org/10.1080/02786826.2017.1383968

[12] Hinds WC, Aerosol technology: Properties, Behavior, and Measurement of Airborne Particles, 1999, Wiley-Interscience Publication.

[13] Hawkes JJ, Coakley WT, Force field particle filter, combining ultrasound standing waves and laminar flow, Sensors and Actuators B: Chemical, 2001, 75 (3), 213-222.

[14] Tuckermann R, Neidhart B, Lierke EG, Bauerecker S, Trapping of heavy gases in stationary ultrasonic fields, Chem. Phys. Lett., 2002, 363 (3-4), 349-354.

[15] Kaduchak G, Sinha DN, Low-power acoustic harvesting of aerosols, IEEE Ultrasonics Symposium Atlanta, 2001.

[16] Goddard G, Martin JC, Graves SW, Kaduchak G, Ultrasonic particle-concentration for sheathless focusing of particles for analysis in a flow cytometer, Cytometry A, 2006, 69 (2), 66-74.

[17] Kaduchak G, Sinha DN, Lizon DC, Novel cylindrical, air-coupled acoustic levitation/concentration devices, Rev. Sci. Instruments, 2002, 73 (3), 1332-1336.

[18] Foresti D, Nabavi M, Poulikakos D, On the acoustic levitation stability behaviour of spherical and ellipsoidal particles, J. Fluid Mech., 2012, 709, 581–592.